International Forum on Aeroelasticity and Structural Dynamics
IFASD 2019-14
9-13 June 2019, Savannah, Georgia, USA

NUMERICAL AND EXPERIMENTAL INVESTIGATIONS ON ACTIVE FLUTTER SUPPRESSION TECHNOLOGIES

Federico Fonte[1], Alessandro De Gaspari[1], Luca Riccobene[1], Francesco Toffol[1], Sheharyar Malik[1], Luca Marchetti[1], Sergio Ricci[1], Paolo Mantegazza[1] and Eli Livne[2]

[1] POLITECNICO DI MILANO, Department of Aerospace Science and Technology
Milano, Italy
(FirstName.LastName)@polimi.it

[2] University of Washington, Seattle, WA 98195 - 2400
eli@aa.washington.edu

Keywords: Flutter Suppression, aeroelastic model, wind tunnel test.

Abstract: This paper discusses the activities carried out during two years of a dedicated project to investigate active flutter suppression technologies and the impact of uncertainties on the expected performances. The investigation is done numerically and through an extended wind tunnel test campaign. Starting from an already available wind tunnel model it is significantly modified to create a new conventional configuration showing a flutter behavior of a typical transport aircraft. The experimental activity has been splitted in two main phases. At first, a half-wing will be tested in a wall clamped configuration to setup the all the hardware components like the flutter controllers based on the aileron, as well the safety devices to avoid breaking the model, in a more manageable configuration. Then, the complete model in free-free configuration has been tested inside the large POLIMI's wind tunnel for the final validation. The paper will describe in details the activities carried out and the experimental results of the wind tunnel test campaign until now.

1 INTRODUCTION

Developments of the capabilities and reliability of aircraft control system hardware and software, combined with the growing structural flexibility, and hence potential for flutter problems and for related weight reduction of optimized composite airframes, seem to have made the implementation of Active Flutter Suppression (AFS) technology closer than ever before [1]. This makes the experimental study of current state of the art AFS important, especially from the perspective of uncertainty, reliability, and the safety of flight vehicles in which this technology will be used.
Contributing to AFS technology development, and to flight vehicle active control in general, for many years, the Politecnico di Milano (POLIMI) developed in the mid-2000s a scaled actively controlled aeroservoelastic model of a three-surface passenger airplane [2-5] and tested it in its large low-speed wind tunnel. Motivated by the need to return to the wind tunnel with an aeroservoelastic model of a configuration that would better capture the aeroelastic behavior of current and emerging commercial passenger and cargo flight vehicles that may benefit from AFS, a research program has been launched by the Politecnico di Milano and the University of Washington to focus on the reliability and safety of AFS-dependent flight vehicles using a wind

tunnel model that would be representative in complexity and aeroelastic characteristic to real aircraft.
The X-DIA aeroservoelastic model has been thoroughly modified, by changes the configuration and by the addition of wind tunnel model features that would allow the study of the effects of uncertainty on the performance and reliability of AFS. The paper describes the modified X-DIA model in detail, regarding configuration, construction, instrumentation, and aeroservoelastic characteristics and will report wind tunnel test results. The paper will serve as a basis for future papers that will report usage of the new model in different active control research efforts and will, hopefully, lead to vibrant active aeroelastic control technology testing using this X-DIA Aeroelastic Wind Tunnel Model.

1.1 Evolution of the X-DIA model

The X-DIA model was originally conceived by POLIMI as a flying platform to investigate many and different topics concerning the flight mechanics, aeroelasticy and active controls. However, with the availability of a new large wind tunnel the model has been transformed from a flying platform to a wind tunnel aeroelastic model. During different EU funded projects different configurations have been developed and tested, but the main architecture, based on three surfaces and forward swept wing never changed. Different wings have been tested with different control surfaces architecture, from a single aileron, to a multi controls configuration (4 leading and 4 trailing edge control surfaces). as shown in Figure 1.

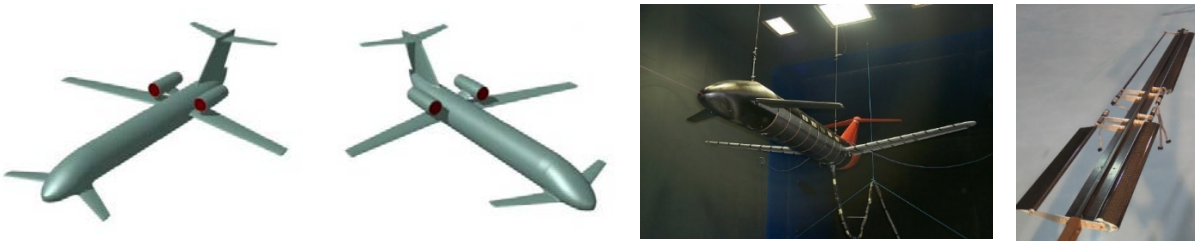

Figure 1: The X-DIA wind tunnel model configurations investigated during the years.

In the framework of AFS project the model has been modified to make it more suitable for the main scope of the project, i.e. to study the flutter suppression technologies and the impact of uncertainties. The updated X-DIA model shows now a more conventional configuration, with a backward swept wing and a T-Tail without the canard (see Figure 1). The structural properties are based on the already available components and, for the new ones, are estimated on the basis of the manufacturing technology adopted, briefly described in the following sections.

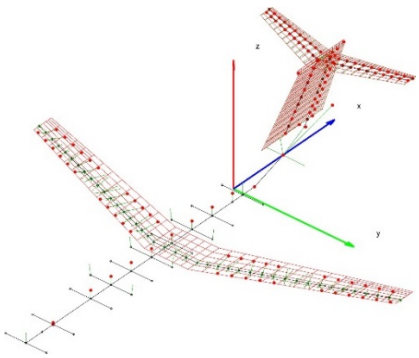

Table 1

Mass	20.8	kg
x_{cg}	-0.389	m
y_{cg}	0	m
z_{cg}	-0.0276	m
I_{xx}	4.976	kgm^2
I_{yy}	12.082	kgm^2
I_{zz}	15.658	kgm^2
I_{xz}	1.519	kgm^2
span	3.0	m
chord	0.25	m

Table 2

$C_{L/\alpha}$	6.13
$C_{mcg/\alpha}$	-4.65
$C_{L/\delta elev}$	0.67
$C_{mcg/\delta elev}$	-3.47

Figure 2: The aeroelastic X-DIA model (left); main characteristics (middle) and stability derivatives (right).

The initial modal analysis showed 20 frequencies in the range 0-45 Hz, while a preliminary trim analysis shows that the model is highly stable, with the most relevant stability derivative (including the aeroelastic correction) are reported in Figure 2. In terms of flutter response, the new X-DIA model shows a classical bending torsional mode around 64 m/s, as reported in the following Figure 3.

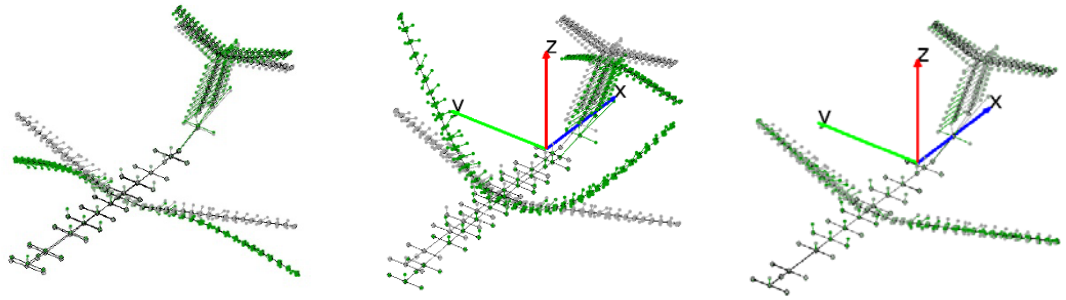

Figure 3: Flutter mode coupling modes 7 and 12 @V_∞=69 m/s (left), structural modes 7 @ 9.08 Hz (center) and 12 @ 12.18 Hz (right), respectively.

2 MODEL MANUFACTURING

The modified configuration of the X-DIA model required the design and manufacturing of new components to replace the original ones. In the following figures the model components are sketched and briefly described.

Structural skeleton

The structural skeleton of the X-DIA wind tunnel model is based on aluminum beams connected together. The fuselage beam is made by an aluminum tube with rectangular section. The main wing spar is made by an omega shape aluminum beam while the horizontal and vertical tails are based on cross shaped aluminum beams. All the structural elements are connected together through aluminum elements properly designed and milled from aluminum blocks. In the rear part of the fuselage a single aluminum frame allows to connect together the TTail assembly and the tailcone to the fuselage main beam (see Figure 4 and Figure 5).

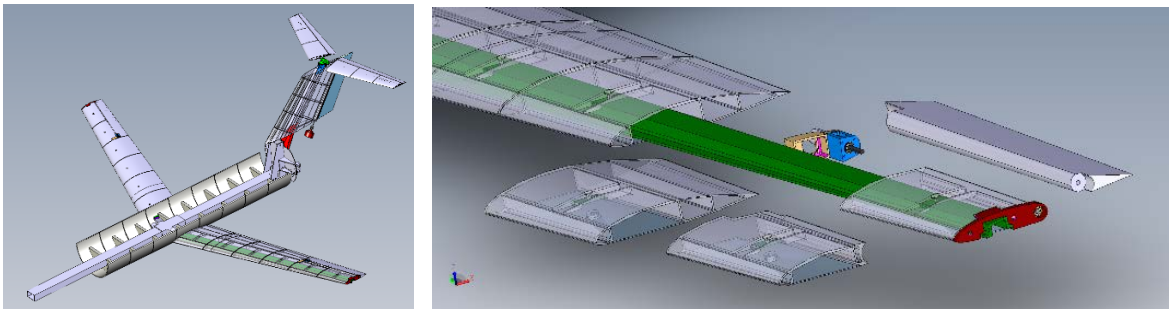

Figure 4: Details of the structural skeleton.

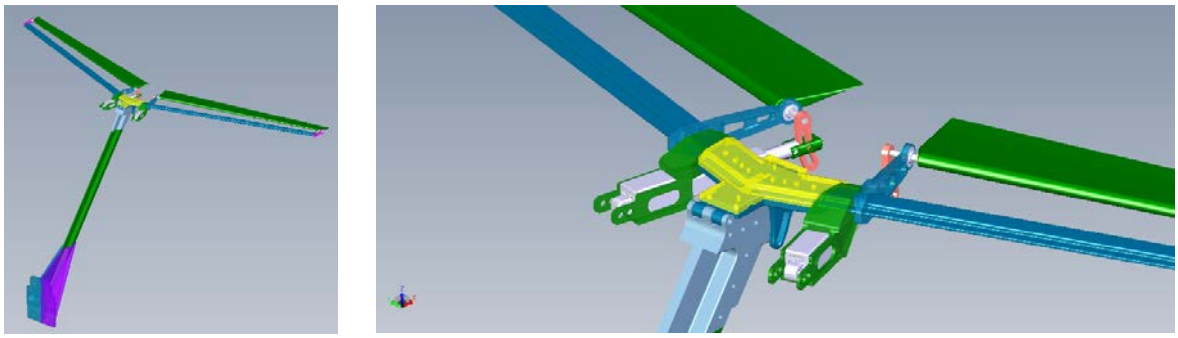

Figure 5: Details of the tail planes including the linear actuators for elevators.

Aerodynamic sectors

The aerodynamic sectors are designed aiming at two main scopes: to guarantee the aerodynamic shapes with enough stiffness and to allow internal space for balance masses and instrumentation installation. Since the contribution of the aerodynamic shape must be limited to the added mass, without altering the stiffness distribution designed for a target aeroelastic scaling, all the aerodynamic sectors are connected to the main beams on a single span-wise location. In the case of the wing and horizontal tail the aerodynamic sectors are manufactured in one shot by 3D printing technology using a special material called XForm that combines high stiffness and low mass and guarantees a very smooth external surface. The wing sectors have been designed to include the elements for the connection to the main spar and, in case of the control surfaces, the hinges and the electric drivers. The aerodynamic sectors of the vertical surfaces are already available, made by Styrofoam covered by carbon fibers. Finally, the aerodynamic sectors of the fuselage are made by honeycomb covered by carbon fibers (see Figure 6 and Figure 7).

Figure 6: The complete wing components just printed out, with details on the cover of the aerodynamic sectors and the aluminum ribs to connect the aileron.

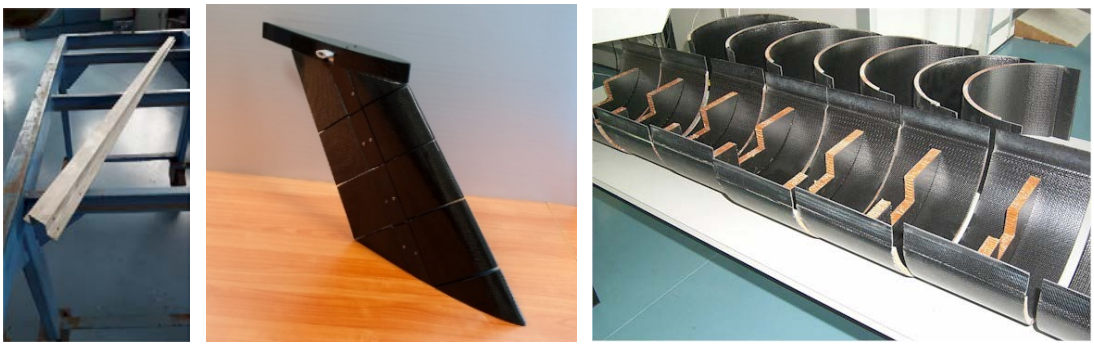

Figure 7: The aluminum wing spar (left), the aeroelastic vertical tail (middle) and the elastic fuselage made by separated carbon aerodynamic sectors made by honeycomb covered by carbon fiber (right).

3 ON-BOARD COMPUTER, SENSORS AND ACTUATION SYSTEMS

The X-DIA wind tunnel model is equipped with two ailerons, that can be actuated in combination or separately, one elevator and one rudder. As usual in the case of wind tunnel model the design of the actuation systems is challenging due to two main requirements: minimum size, so to be installed inside the wing airfoil thickness, and the allowable bandwidth, allowing to control the most relevant modes. The control system of ailerons and rudder is based on RSF-5B and RSF-9B by Harmonic Drive electric motors, respectively, connected to the control surfaces by means of elastic joints. In the case of the elevator, a similar solution has been adopted but based on a single linear actuator moving together the right and left elevator. A PID controller based on two possible configurations, i.e. single and double loop, has been designed and adopted aiming at two requirements: the possibility to introduce the saturations typical of full scale aircraft actuators, and a maximum bandwidth of at least 15 Hz. The two elevators are driven by two Actuonix L-16 linear actuators that shows a limited bandwidth ut this is not considered a limitation since no active control lows based on the use f elevators are foreseen in the project. The main sensors will be MEMS accelerometers by PCB selected for their good accuracy at low frequencies but mainly because being already pre-amplified the corresponding channels can be read by a standard data acquisition system without the need of expensive and heavy IEPE modules usually adopted in case of piezo-electric accelerometers. This choice allows for a selection of a small embedded computer to be installed inside the model and able to completely manage the test in terms of acquisition and active control duties. The embedded computer is equipped with the in house developed RTAI Real Time operating system based on Linux. The embedded computers as well all the necessary acquisition cards are based on the PC-104 form factor allowing for a final small size and weight embedded system (see Figure 8 and Figure 9).

a b c d

Figure 8: The Aries PC-104 from Diamond (a), the MEMS PCB accelerometer (b), the Actuonix L16-S Miniature Linear Actuator (c) and the Harmodic Drive motors for aileron and rudder control (d).

Figure 9: The box containing the drivers for the electric actuators (left) and the complete onboard computer equipped with all the requested I/O cards (right).

4 TWO-PHASES WIND TUNNEL TEST STRATEGY

To simplify the wind tunnel test campaign, as well as to decrease the complexity of the test due to the many parameters and potential uncertainties involved, it was decided to split the wind tunnel campaign in two phases: in the first one the half wing, in clamped configuration, will be tested for a correct identification of the flutter velocity and to setup the sensors and data acquisition system as well the controllers. This test will be carried out into the Department Wind Tunnel, equipped with a test chamber of 1.5x1x3m and a maximum velocity of *55 m/s*. Then, the full X-DIA model will be tested in a free-free configuration in the POLIMI's large wind tunnel. This is based on a unconventional configuration, i.e. a closed circuit where the return circuit is used for wind engineering tests with a large testing room sizing 4x14x34m. Two moving test chambers for aerospace testing are available, sizing 4x4x6m with a maximum speed of *55m/s*. Despite the low Mach number, the large size of the chamber allows to test large scale models (see Figure 10).

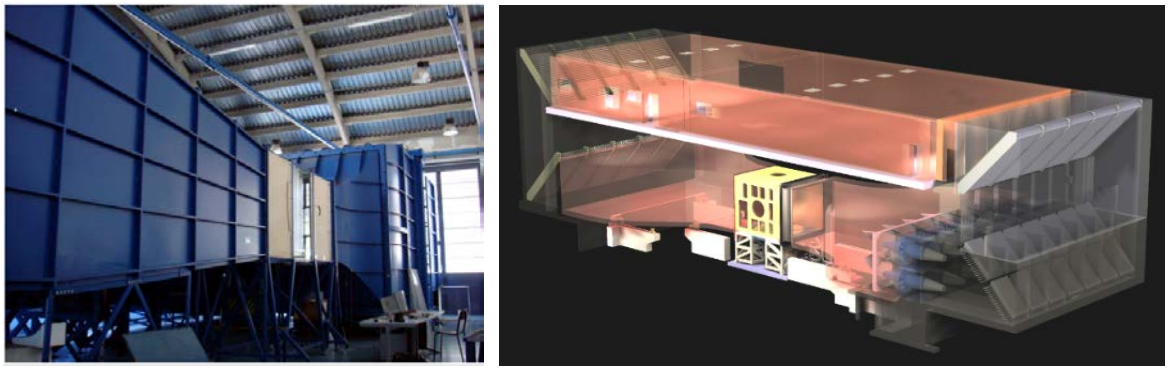

Figure 10: The Department Wind Tunnel (left) and the POLIMI's Large Wind Tunnel (right).

5 PHASE I: THE HALF WING CONFIGURATION

The PHASE 1 of the activity focused on the X-DIA wing only, in clamped configuration, and includes the finalization, GVT and modal correlation, as well the numerical design of the active flutter suppression contreller and its final wind tunnel validation.

5.1 Modal analysis and numerical vs. experimental correlation

Following the strategy adopted for the test campaign, a detailed numerical model has been developed for the half wing that, after the numerical convegence cheks, has been validated by means of a Ground Vibration Test session, carried out in free-free configuration (see Figure 11).

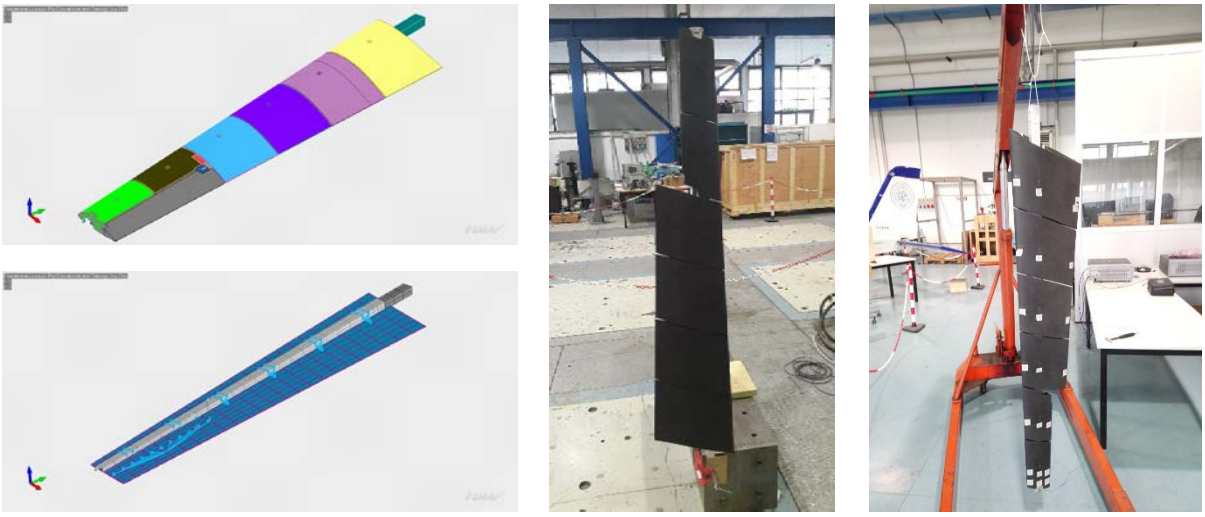

Figure 11: The half wing numerical model and the setup during the ground vibration test.

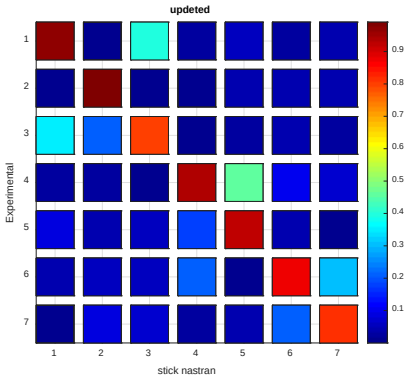

Numerical (Hz)	Exp (Hz)	Err (%)	Shape
8,26	8,29	-0,63	1th Out plane
9,71	9,56	1,6	1th In Plane
19,83	20,01	-0,92	1th Torsion
37,53	38,40	-2,26	2nd Bending
49,26	52,44	-6,06	-
61,81	61,31	0,84	2nd Torsion
66,83	74,40	-10,17	-

Figure 12: The Cross MAC matrix (left) and the comparison between the updated numerical and experimental frequencies (right).

One of the relevant results of the final modal updating, as reported in Figure 13, on the basis of the experimental modal analysis results, is a significant variation of the original frequencies but, most important, a decrease of the in-plane mode that is now the second mode, with higher frequency of the first out of plane bending and lower than the first torsion. This aspect could be believed not so important, since usually the in-plane mode is not associated to any aerodynamics contribution, at least if unsteady aerodynamic calculation is done with the classical DLM approach. However, in this case the situation is different. Indeed, the wing spar is based on an open Omega shape section, meaning that the elastic axis is outside the section itself, outside the wing plane. This situation creates a dynamic coupling leading to a torsional-in-plane-bending vibration mode with relevant consequences on the flutter behavior.

5.2 Flutter Prediction

As anticipated in previous section, the main consequence from the flutter point of view of the in-plane – torsion coupling is that the wing does not show the typical bending-torsion flutter mode, but a more complex mechanism, involving three modes at the same range of velocity. To try reducing the coupling a small modification has been introduced, by placing an appropriately designed tuning mass, of about 160 g, on a small winglet, actually a simple plate, placed outside the wing plane (see Figure 14). In such a way the wing mass axis is brought as

close as possible to the elastic axis. Even if, at least numerically, it is possible to completely remove the dynamic coupling, In the practical situation there remains a small coupling. In the following Figure 15 depicts V-g plots, with and without tip mass.

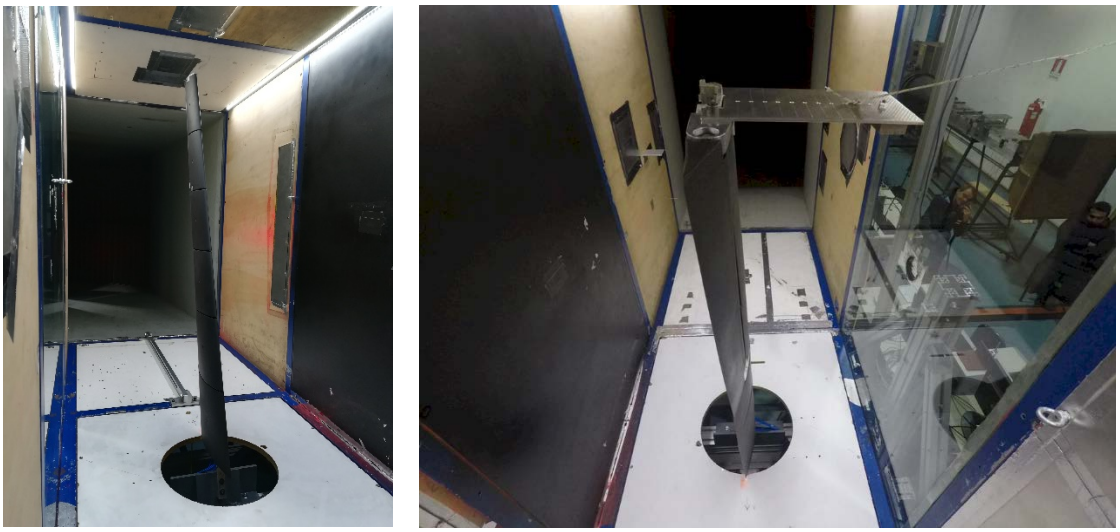

Figure 13: The wing installed in the wind tunnel (left) and the winglet equipped with the balancing mass (right).

The flutter analysis shows results similar to ones already obtained during the preliminary analysis of the full model, with a flutter velocity simply tunable by means of small masses added to the wing tip.

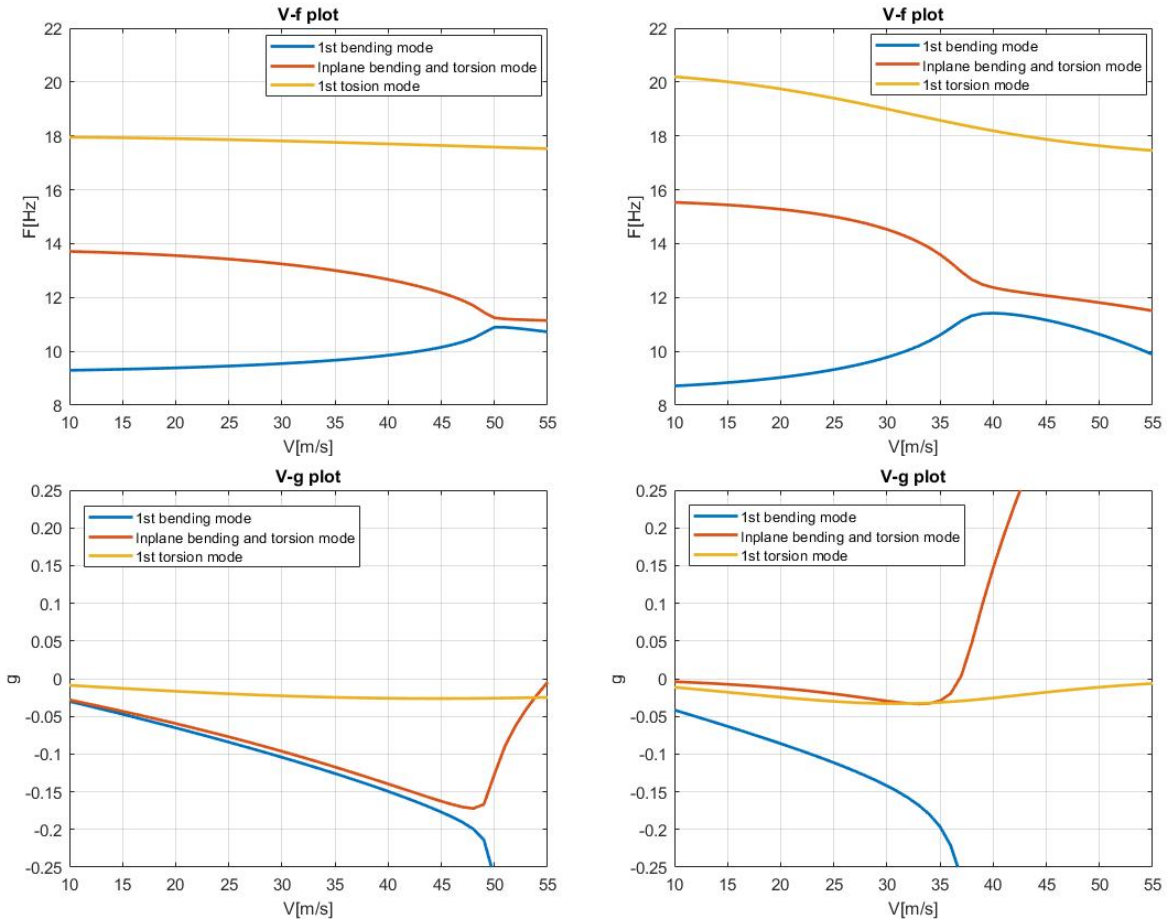

Figure 14: V-g plots of clamped half-wing with a 50 g mass on the tip in forward (left) and rear (right) position.

5.3 The Servo Controller

While the aircraft are usually equipped with actuation systems realized by means of electro-hydraulic actuators that show various saturating behaviors in the case of wind tunnel models, due to the constrained in size, small electrical motors are usually adopted to actuate its control surfaces. This is the case of X-DIA model also, as reported in Section 3. Since these motors do not present any position saturation, the typical real system saturations in terms of maximum rotation and rotation velocity are implemented by adopting a dual loop approach based on PID controllers is implemented. The inner controller Ci of the motor loop is designed as a PI speed controller, making the actuator sufficiently fast to follow abrupt speed changes, e.g. possible rate saturations. The output controller Co of the load (outer) loop is implemented as a PID position controller, in order to assure the desired positioning precision within the required bandwidth, in this case *20 Hz*. A sketch of the servo controller is sketched in Figure 16.

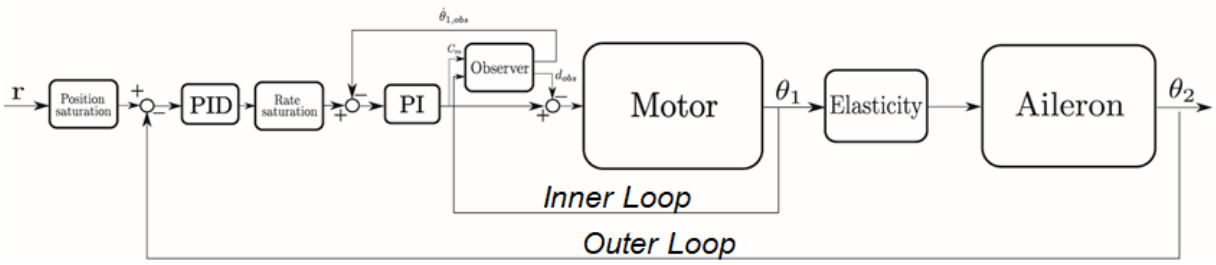

Figure 15: The dual loop controller scheme adopted to implement the requested saturations on the aileron's electric motors.

5.4 Active Flutter Suppression Controller Design

Inside AFS project two different strategies have been followed in terms of flutter control strategy. The first one, implemented by POLIMI, is based on the idea to design a very simple while robust control system that do not require an extended campaign to identify and tune the different parameters related to the aeroservoelastic systems. The second one, implemented by UWA, is based on the use of modern robust control techniques. In this paper only the first strategy is detailed.

The flutter suppression control scheme has been developed aiming at these goals:

- Simple, direct feedback controller (accelerations and velocities)
- Limited number of feedback sensors (4 accelerometers)
- Optimal definition of control gains to guarantee control robustness by means of a multi-model design, including different velocities and uncertainties on servo-controller properties

The design of the controller is formulated as an optimization problem (nelder mead global optimization) aiming at minimize the peaks of the two modes involved in the flutter, i.e. bending and torsion modes. Starting from modal and aeroelastic matrices (Mhh, Khh, Qhh) extracted by Nastran (SOL103 and SOL145), eigenvalue problems are solved for different speeds within the range of interest (*30-60m/s*) and the algorithm finds control gains (G_{11}, G_{22}, G_{33}, G_{44}, G_{55}, G_{66}, G_{77}, G_{88},) to minimize the maximum peaks amplitude. The main characteristics of this approach are the following:

Multi-model method: the maximum amplitude is computed considering different models obtained for different model perturbations, at each optimization step.

Structured robustness included in the design: different model perturbations.

1. Different speeds (*30-60m/s*);
2. Different parameter sets of the servo control (Outer loop PID and Inner loop PI gains);

Structured robustness included during the verification phase

1. Random perturbations (75%-125%) of modal and aeroelastic matrices;
2. Perturbation of mode frequencies.

In the following Figure 16 the scheme of the adopted procedure as well the Frequency Response Function of the wing tip acceleration in open and closed loop are reported, respectively, showing the corresponding variability bands.

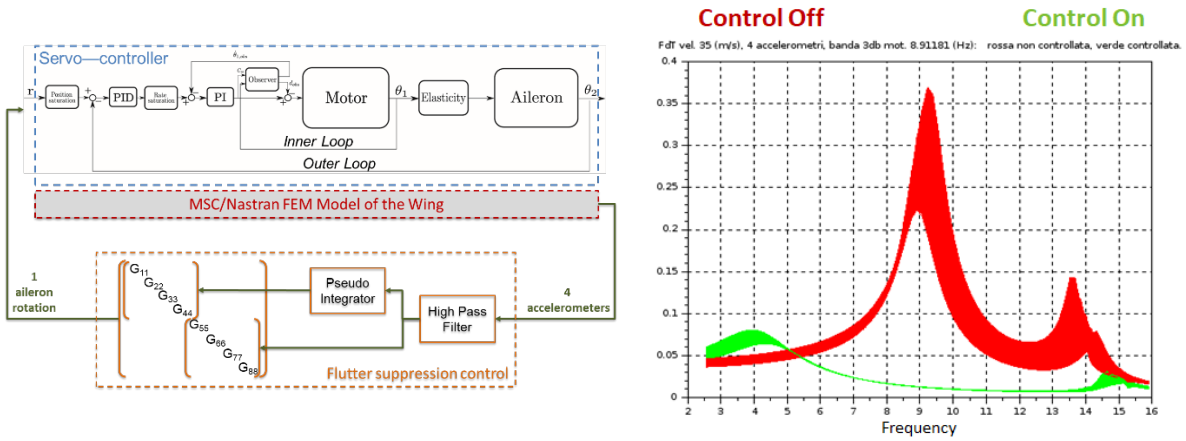

Figure 16: The active flutter suppression scheme (left) and the numerical robustness analysis results (right).

5.5 Experimental Flutter Identification

To conclude the PHASE I wind tunnel test campaign, two different activities have been carried out, i.e. the flutter identification, to be compared with the numerical simulations, and second the flutter suppression test.

The first preliminary experimental campaign has been carried out November 2018 aiming at getting confidence on the flutter prediction capability of the numerical FEM model. The half wing model has been installed on the Department Wind Tunnel in a vertical position, clamped at the tunnel floor. Ten monoaxial MEMS accelerometers were embedded into the wing to identify frequencies and mode shapes. The excitation of the wing during the flutter test has been produced by the wing aileron, excited with a *2.0 degs* amplitude linear sinusoidal sweep, covering in a range *5-20 Hz* in 30 seconds (see Fig. 19). A manually actuated safety device has been implemented to stop the wing in case of divergent flutter. However, when its power in stopping an oscillation was tested, at the relatively high speed of *47.5 m/s*, it turned out to be a flutter generator. In fact, the readily found mass of 2 Kg, attached at the wind tip and close to the symmetry line of the longeron, was too small to provide a constraint and became a flutter tuning device. The test has been completed in two incremental steps from *0-30 m/s* and from *30* to *47.5 m/s* followed by two identification phases so to predict the flutter velocity in a safe way and to limit the risk of losing the wing model. He wing is excited by an aileron sweep with amplitude *2 degs* in the bandwidth *5-50 Hz*, for a duration of *30 s* (see Figure 16). Figure 17 shows the evolution of one the accelerometer on the wing tip with the increasing velocity. It very easy to recognize the typical flutter trend characterized by the coalescence of the bending and torsion peaks, whereas, contrarily to straight wings, it is the bending peak that emerges against a disappearing torsional mode.

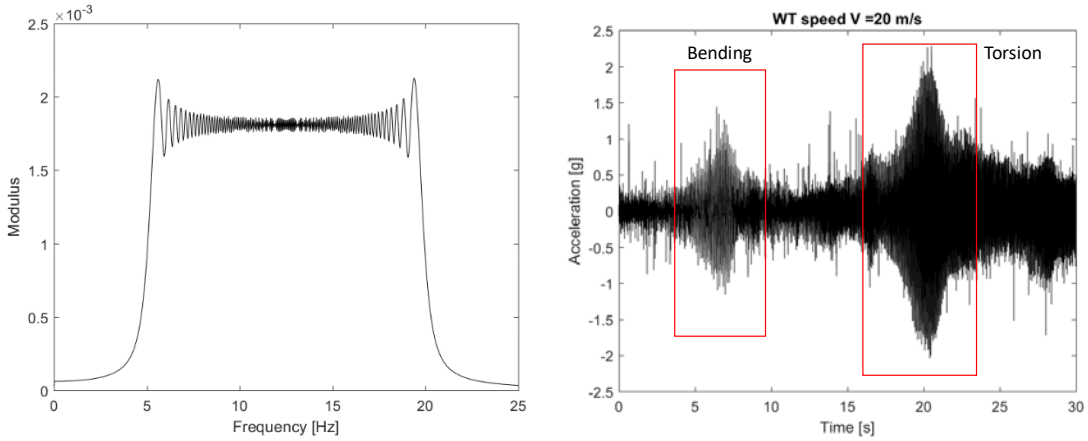

Figure 17: Aileron sweep spectrum (left) and typical time history of one of the accelerometers located on the wing tip (right).

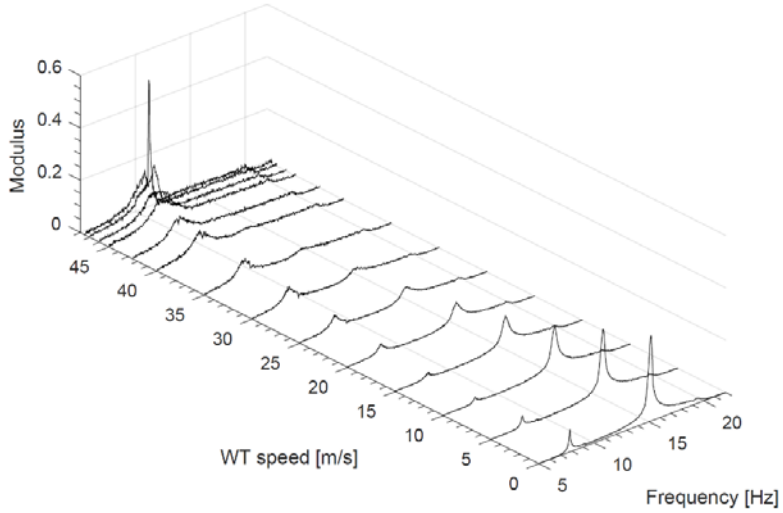

Figure 18: Evolution of the tip acceleration with the increasing test velocity.

Figure 20 shows the identification results. Four different identification methods have been applied, i.e:

1) an SISO ARX identification in the time domain [14], which is then used just for reconstructing the related transfer function, whose poles as then identified in the frequency domain;

2) the Polyreference approach [15], as implemented in the well-known TestLab software from Siemens, formerly LMS, whose results are then used as a starting solution for an MLMS refinement;

3) A full time domain SISO ARX [13], providing the model aeroelastic eigenvalues by directly computing the zeros of the discrete autoregressive part, which are then converted to their continuous parents, along with the determination of their uncertainty.

4) the same as for 3, but with an ARMAX model.

Due to their capability of better modeling unknown external disturbances, the approaches 3 and 4 where expected to provide a somewhat improved identification. However, due to the fairly smooth wind tunnel flow, a good level and frequency content excitation and a low noise instrumentation, the computed poles uncertainties provided by 3 and 4, showed that any of the used methods was quite adequate for predicting the flutter point from a simple extrapolation of the already available V-g plot.

The accuracy of the identified results is well shown from the V-g plot below, whereas, from an engineering point of view, substantially equivalent trends and a somewhat hard flutter are provided by the used approaches. The highest velocity tested was *47.5 m/s*, very close to the

predicted flutter velocity, so to identify at least one point on the steep damping decrease of the curve tracking the evolution of the null damping torsion mode. Finally, the flutter mode shape is reported in Figure 21, as well as the Gauss plane of the identification results, showing the almost uncoupled in plane mode.

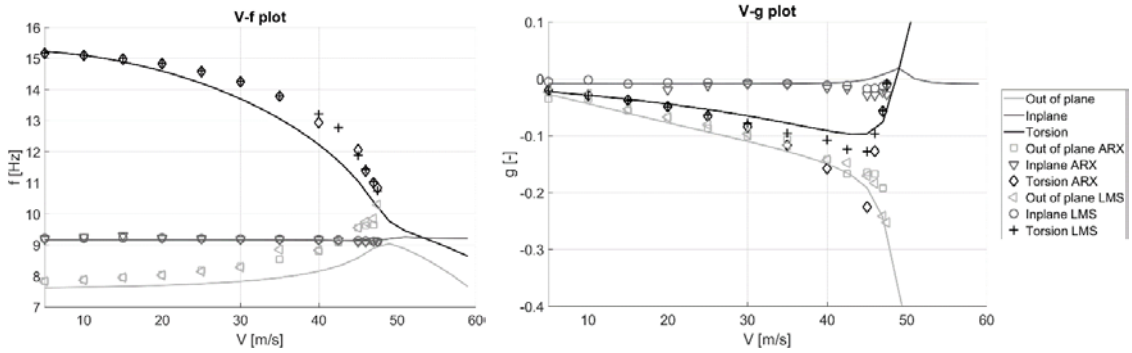

Figure 19: V-g plots reporting the numerical estimations and the identification results.

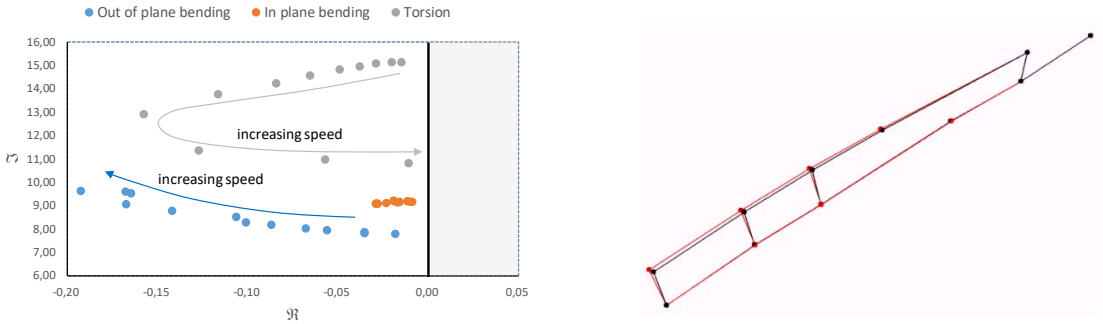

Figure 20: Identification results (LMS method): The Gauss plane (left) and the flutter mode corresponding to 47.5 m/s.

5.6 Flutter Suppression Validation

After the identification phase the active flutter controller has been verified in a dedicated wind tunnel test session. Different runs have been performed by small increasing of the wind tunnel speed so to approach the predicted flutter speed, to check the open as well the closed loop configurations. Figure 22 show two test sequences taken at *42.5* and *47 m/s* where the model is excited by the aileron sweep already adopted during the identification phase, in a sequence of control off and on.

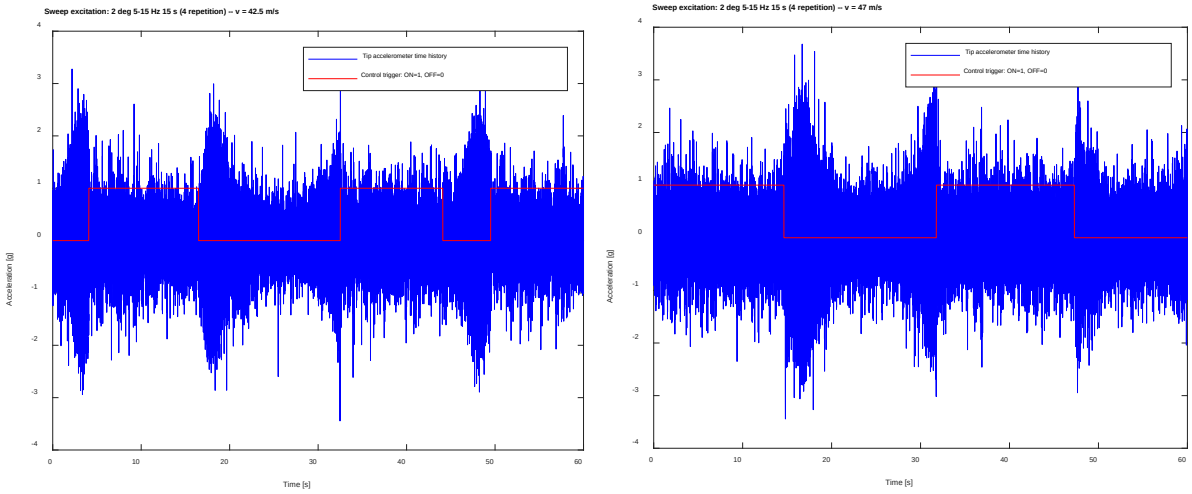

Figure 21: Preparatory sweep to check the active flutter suppression system approaching the expected flutter point.

After this run up phase, the active flutter control has been switched on and the wind tunnel speed increased up to *50 m/s*, so passing the estimated flutter speed. The control worked properly to control the wing responses, as shown in Figure 23 where the aileron's rotation as well the tip acceleration is reported for a total measurement time of about *55* seconds.

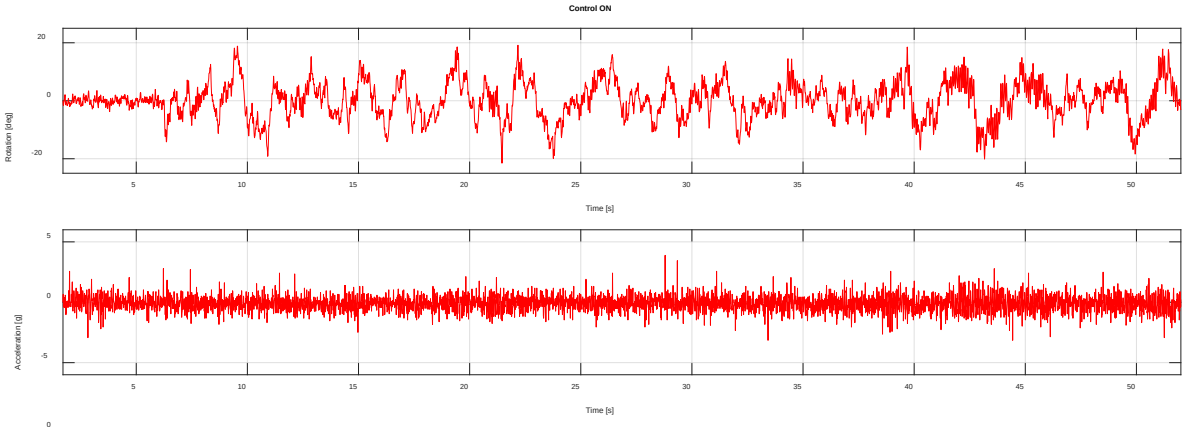

Figure 22: Measurements taken at *V=50 m/s* demonstrating that the flutter is successfully controlled.

6 PHASE II: THE COMPLETE X-DIA MODEL CONFIGURATION

Once completed the activity on the clamped wing, the complete X-DIA model has been finalized and tested in the Large POLIMI's Wind Tunnel. This section summarizes the activities completed aiming at this final test.

6.1 GVT results on the complete X-DIA model, modal correlation and modal updating

The GVT has been carried out on the complete X-DIA model equipped with all the relevant hardware components, such as sensors and wiring, simulating the expected weight of the complete onboard computer and drivers for electric actuators by dummy masses. The model has been suspended by means of two soft springs connected to the fuselage and excited by hammer impacts. A total of 110 accelerometers was used for modal identification. Some pictures taken during the GVT are shown in Figure 24 and Figure 25.

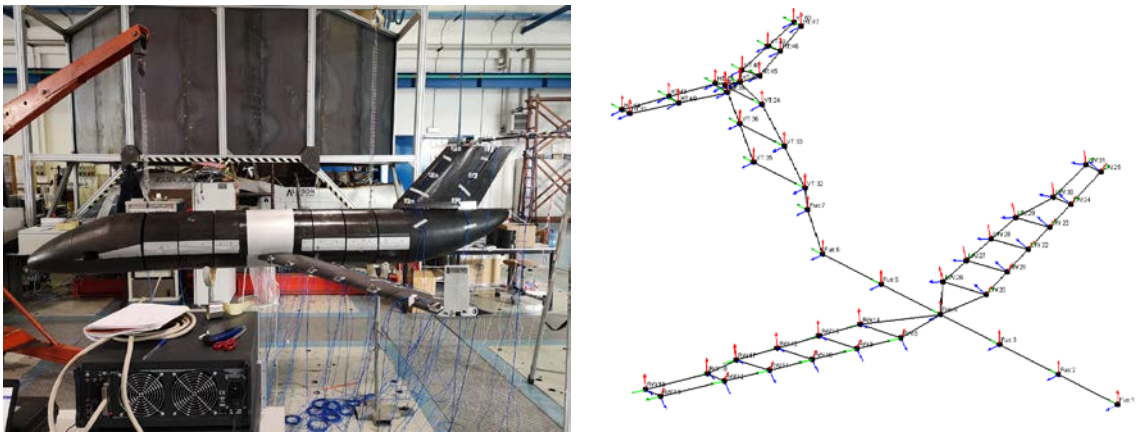

Figure 23: The GVT of the complete X-DIA model (left) and the experimental mesh adopted (right).

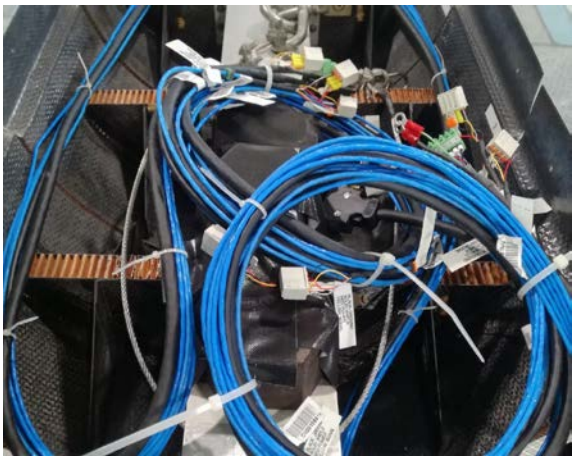


Figure 24: Dummy masses to simulate the presence of the onboard computer and electric motor drivers (left); details of the struts added to increase the stiffness of the connection ot the T-Tail connection (right).

GVT	Initial FEM	Err.	Updated FEM	Err.	Shape
Hz	*Hz*	*%*	*Hz*	*%*	
7,55	8,10	7,3	8,27	9,5	Vtail torsion + htail antisymmetric bending
7,67	8,37	9,1	7,89	2,9	**Wing + htail symmetric bending**
9,12	8,74	-4,2	8,95	-1,9	Vtail bending + htail antisymmetric torsion
10,83	19,51	80,1	10,93	0,9	Htail symmetric bending
13,66	13,47	-1,4	13,38	-2,0	Wing + htail antisymmetric in-plane bending
13,82	12,56	-9,1	13,13	-5,0	**Wing in-plane symmetric bending and torsion + htail in and out-of-plane bending**

Table 3

The GVT results have identified the TTail connection as well the Htail as too weak. To solve this issues two actions have been decided: to install two extra struts connecting the Htail to the main spar of the Vtail and second to design and manufacture a new spar for the Htail made in steel in place than aluminum. This second action will be implemented for the final flutter test campaign. Due to these issues, the updating activity was mainly concentrated on matching the most relevant modes involving the wing and highly participating in the flutter phenomenon, as reported in Table 3.

6.2 Flutter Prediction

The flutter prediction of the complete X-DIA model has been carried out running the classical SOL 145 of Nastran using the updated dynamic model. In this configuration the aeroelastic model shows two main flutter around *43* and *47 m/s* (see Figure 26), showing the coupling between the first wing bending and the first wing torsion symmetric and antisymmetric, respectively (see Figure 27).

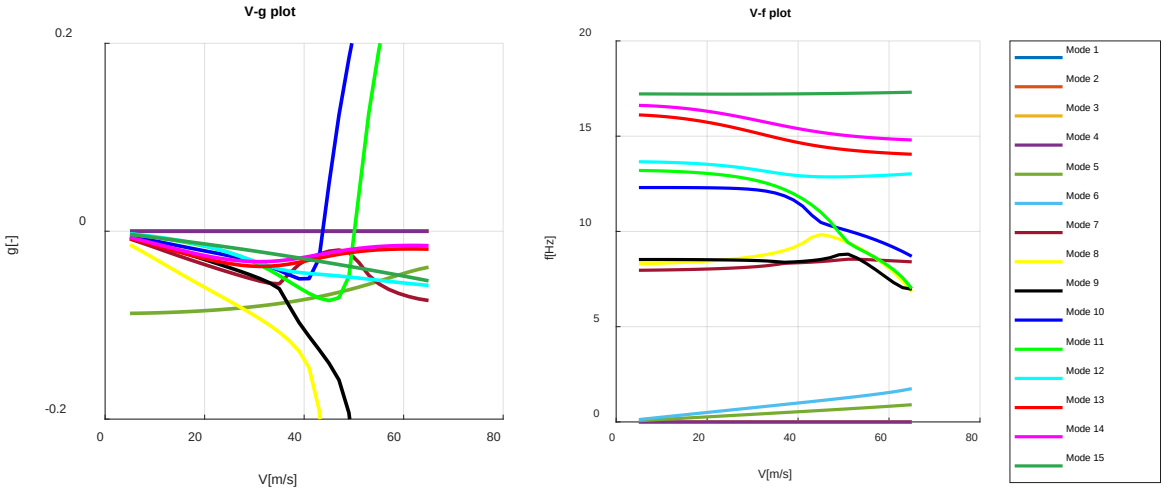

Figure 25: The predicted flutter behavior on the basis of the updated dynamic model.

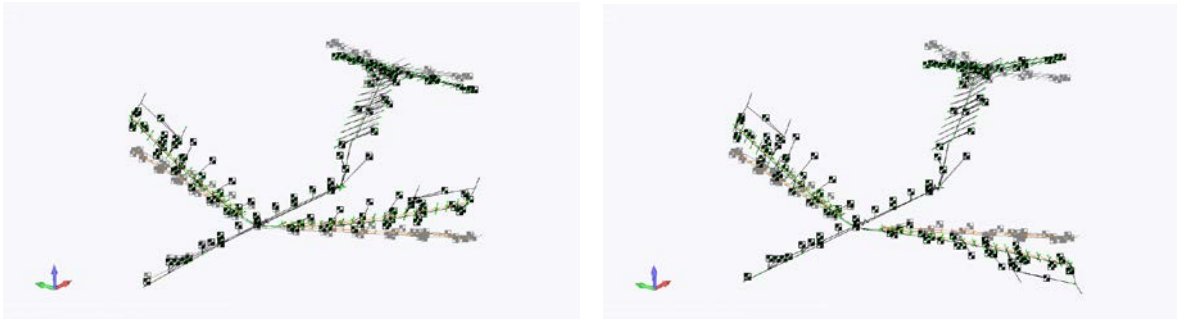

Figure 26: The two modes involved in the first flutter phenomena: first symmetric wing bending (left) and first asymmetric torsional mode (right).

6.3 Shakedown Wind Tunnel Test on the Complete X-DIA Model

The first wind tunnel test campaign on the complete X-DIA model in the large POLIMI's Wind Tunnel has been carried aiming at testing the complete model setup, verify the functionality of all the onboard systems and identify the flutter parameters. The model was suspended in a controlled free-free configuration, by means of two series of cables connecting the wings to the side walls of the test chamber, the fuselage on the roof and one very long anti-drag cable connecting the nose of the model to the convergent section of the wind tunnel (see Figure 28) The model was equipped with 20 MEMS mono axial accelerometers plus one capacitive triax accelerometer located on the CoG. The aileron rotations are measured by means of the embedded encoders.

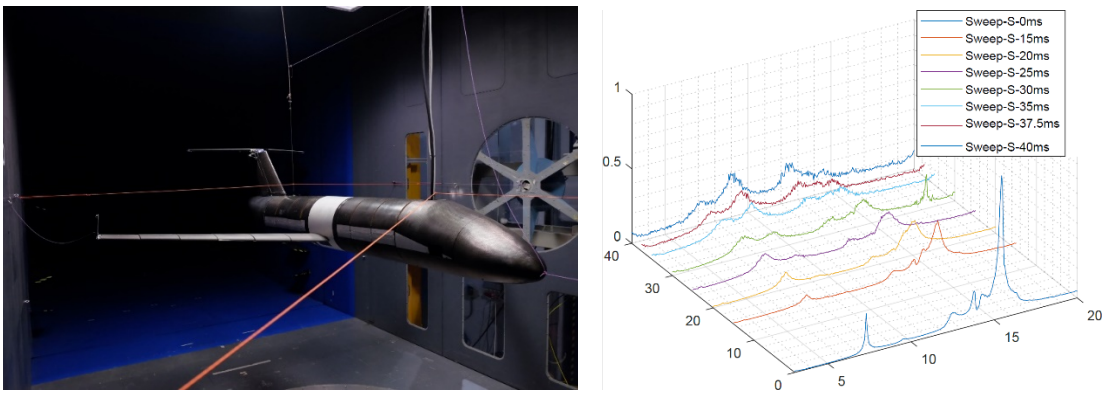

Figure 27: The adopted setup inside the large POLIMI's Wind Tunnel (left), typical FrF envelope of tip accelerometer for increased velocity.

The finalization of the suspension system requested some extra masses that were not considered in the previous GVT, meaning that a frequency shift was expected during the flutter identification phase. Due to the goals of this test campaign this model variation has been considered as acceptable. The model was excited with symmetric and antisymmetric aileron's sweep in the bandwidth *5-30 Hz* at *10, 20 30* and *40 m/s*, using a decreasing amplitude from *5* to *2 degs* from the lower to the higher velocities. In terms of flutter identification, the same approaches already used for the clamped wing have been applied. Figure 29 shows the results obtained demonstrating an acceptable correlation level in terms of damping factor despite the expected frequency shift.

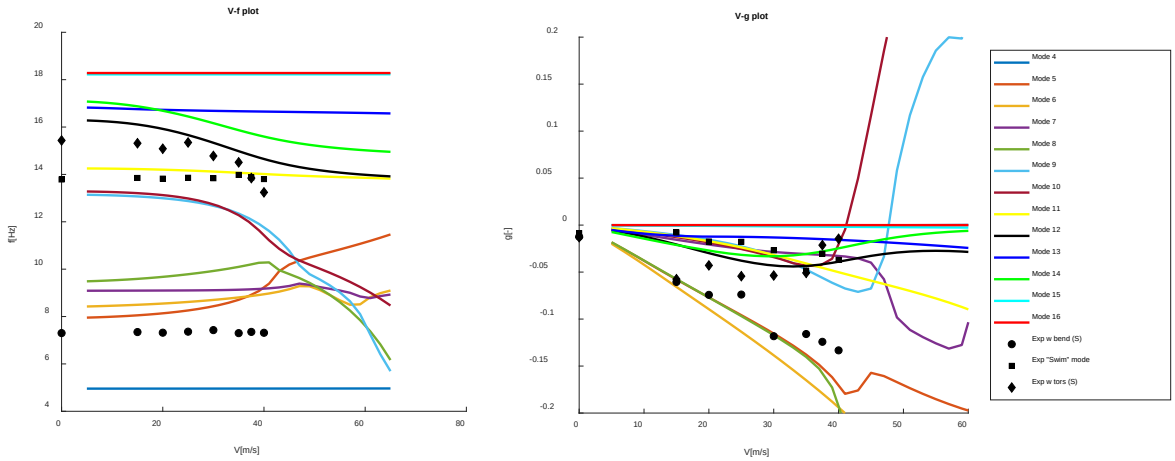

Figure 28: Numerical vs, experimental flutter identification results after the first test of the complete X-DIA model in the Large POLIMI's Wind Tunnel.

6.4 Safety Anti-Flutter Device Design and Implementation

In preparation of the final flutter suppression test, in order to limit the risk of braking the model in case of a non-properly working of the flutter suppression system a safety device has been designed. It consists in a pneumatic actuator simple installed on the wing tip able to move a small mass from the trailing edge to the leading edge position (see Figure 30). A series of numerical simulations have been carried out to finalize the dimensions of the device as well the mass value of the moving mass. Thanks to the presence of the device, the flutter mechanism has been changed, showing now the flutter velocity around *43 m/s* with the mass in the rear position, and far away and outside the wind tunnel velocity range with the mass in the forward position (see Figure 31 and Figure 32).

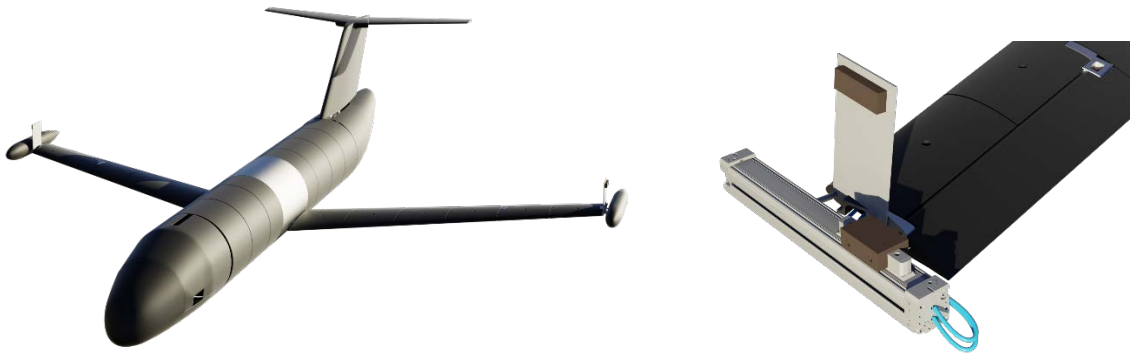

Figure 29: Finalized X-DIA model including a tip anti-flutter safety device.

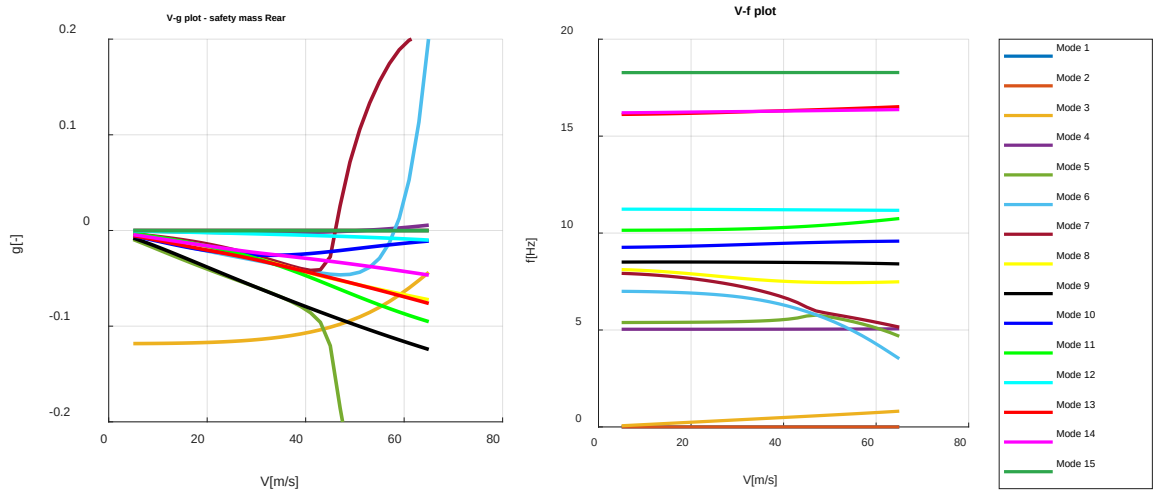

Figure 30: Numerical V-g plot including the anti-flutter device: tip mass in rear position, V_F= *43 m/s*.

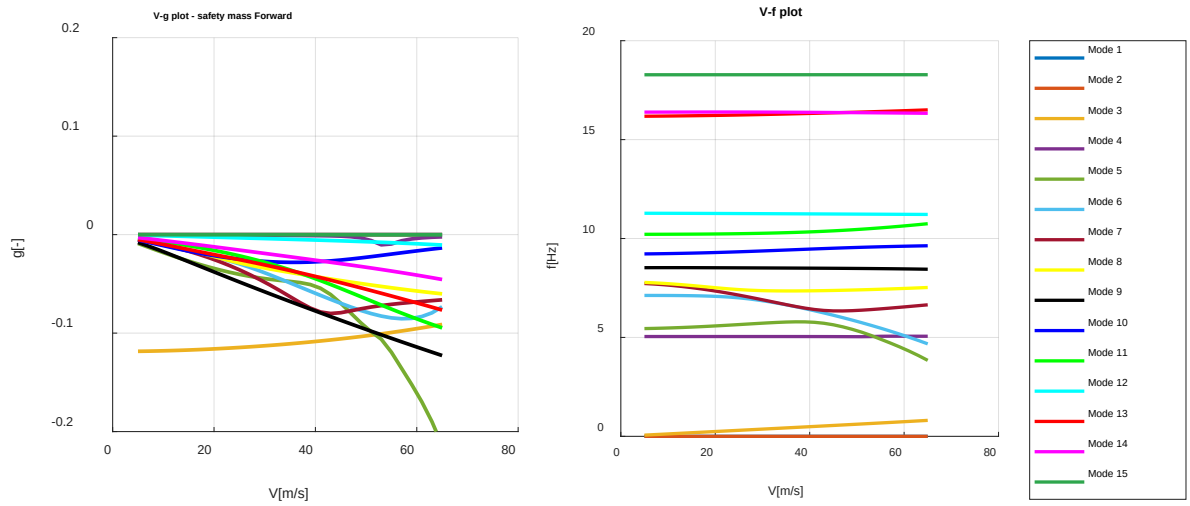

Figure 31: Numerical V-g plot including the anti-flutter device: tip mass in forward position: no flutter.

7 CONCLUSIONS

The paper summarizes the activities carried out in the framework of AFS project, aiming at the experimental characterization and control of typical wing flutter. The main scope of this research activity is the validation of flutter control technologies and the investigation of the impact of uncertainties on their performances. Aiming at this high level target, a *3m* span fully aeroelastic wind tunnel model has been designed and manufactured, by modifying a previously available model called X-DIA. Due to the complexity of the activity, a two stages testing strategy has been adopted. In the first phase the flutter test has been carried out on a half-wing in a small size wind tunnel, to check the prediction capabilities as well the numerical models available. In a second phase the flutter test will be carried out on the complete model, in free-free configuration, inside the large wind tunnel of POLIMI.

The paper reports the results of the so called PHASE I experimental campaign aiming at the implementation and validation of the active flutter suppression system for the clamped wing configuration. The results obtained demonstrated the validity of the hardware platform and the capability of the simple controller here proposed to suppress the wing flutter.

Then, the activity aiming at the full model finalization as well the results of the first shakedown test performed in the Large POLIMI's Wind Tunnel have been reported. The model, and especially the instrumentation and onboard data acquisition system and controllers appeared as

very reliable allowing to completely manage the test remotely from the control room. The flutter identification results confirmed the numerical predictions. Finally, a dedicated anti-flutter device has been designed to conduct the final PHASE II test session, scheduled for July 2019, with an acceptable level of safety.

8 REFERENCES

[1] Livne, E, “Aircraft Active Flutter Suppression: State of the Art and Technology Maturation Needs”, Journal of Aircraft, Vol. 55, No. 1, Jan.-Feb. 2018, pp. 410-452, doi: 10.2514/1.C034442.

[2] Sergio Ricci and Alessandro Scotti. "Aeroelastic Testing on a Three Surface Airplane", 47th AIAA/ASME/ASCE/AHS/ASC Structures, Structural Dynamics, and Materials Conference, Structures, Structural Dynamics, and Materials and Co-located Conferences. Newport, Rhode Island. 2006.

[3] Sergio Ricci and Alessandro Scotti. "Aeroelastic Testing on a Three Surface Airplane", 47th AIAA/ASME/ASCE/AHS/ASC Structures, Structural Dynamics, and Materials Conference, Structures, Structural Dynamics, and Materials and Co-located Conferences. Newport, Rhode Island. 2006.

[4] De Caspari, A., Ricci, S., Riccobene, L., and Scotti, A., "Active Aeroelastic Control Over a Multisurface Wing: Modeling and Wind-Tunnel Testing", AIAA Journal, 2009, Vol.47, pp.1995-2010, doi: 10.2514/1.34649

[5] Ricci, S., Scotti, A., Cecrdle, J., and Malecek, J., “Active Control of Three-Surface Aeroelastic Model”, Journal of Aircraft, 2008, Vol.45, pp. 1002-1013, doi: 10.2514/1.33303.

[6] Mattaboni, M., Quaranta, G., and Mantegazza, P., “Active Flutter Suppression for a Three-Surface Transport Aircraft by Recurrent Neural Networks”, Journal of Guidance, Control, and Dynamics, 2009, Vol.32, pp. 1295-1307, doi: 10.2514/1.40774

[7] M.Lanz, S.Ricci, “Progetto di un Modello Radiocomandato per Prove Aeroelastiche in Volo”, Dipartimento di Ingegneria Aerospaziale, Memoria n. 92-32, 1992.

[8] Ghiringhelli G., Lanz M. and Mantegazza P., "A comparison of methods used for the identification of flutter from experimental data", Journal of Sound and Vibration, Volume 119, Issue 1, 22 November 1987, Pages 39-51.

[9] L. Ljung, System Identification;Theory for the User, 2nd Ed., Prentice-Hall, 1999.

[10] Bart Peeters, Herman Van der Auweraer, Patrick Guillaume, and Jan Leuridan, “The PolyMAX Frequency-Domain Method: A New Standard for Modal Parameter Estimation?” Shock and Vibration, vol. 11, no. 3-4, pp. 395-409, 2004. https://doi.org/10.1155/2004/523692.

[11] S. Ricci, F. Fonte, A. De Gaspari, L. Riccobene, P. Mantegazza, F. Toffol and E. Livne, “Development of a Wind Tunnel Model for Active Flutter Suppression Studies”, AIAA Scitech 2019 Forum, 7-11 January 2019, San Diego, California, https://doi.org/10.2514/6.2019-2029

ACKNOWLEDGEMENT

Support by the Federal Aviation Administration as well as contributions by Wael Nour and Sohrob Mottaghi from the FAA are gratefully appreciated. A special thanks to Mauro Terraneo from Vicoter for his continuous support during the modal identification phase.

COPYRIGHT STATEMENT